Engineering Journal issn: 0125-8281

Article

Efficiency of Heat Transfer Improvement Performed in Circular Tubes Utilizing Various Types of Ring-Shaped Turbulators

Chotitach Jitbumrung[1,a], Chayanoot Kositanont[2], Suttichai Assabumrungrat[2], and Sompong Putivisutisak[1,b,*]

1 Advanced Computational Fluid Dynamics Research Unit, Department of Mechanical Engineering, Faculty of Engineering, Chulalongkorn University, Phayathai, Bangkok 10330, Thailand
2 Center of Excellence in Catalysis and Catalytic Reaction Engineering, Department of Chemical Engineering, Faculty of Engineering, Chulalongkorn University, Phayathai, Bangkok 10330, Thailand
E-mail: [a]chotitach.j@gmail.com, [b,*]sompong.pu@chula.ac.th (Corresponding author)

Abstract. The enhancement of heat transfer performance by using different types of ring-shaped turbulators equipped in a circular tube was investigated through 3D numerical simulations (CFD) with the finite volume method. Three types of turbulators—orbicular-ring turbulator (ORT), pyramidal-ring turbulator (PRT) and proposed innovative cogwheel-ring turbulator (CRT)—were considered. Air at 300 K was passed through the tube with uniform wall heat flux conditions varying from Reynold's numbers of 4,000 to 20,000. The standard $k-\varepsilon$ turbulence model was used to simulate the flows via the ANSYS FLUENT commercial software. Geometric influences in the heat transfer were investigated in terms of compositing the diameter ratio (DR = 0.5, 0.6 and 0.7), the pitch ratio (PR = 4 and 8) and the number of teeth in the cogwheel-ring turbulator (N = 6, 8 and 10). In conclusion, the heat transfer rate in the tubes fitted with ORT and PRT were in the range of 87, which was 199% higher than that of the tube without a turbulator. The PRT offered a slightly higher heat transfer rate than the ORT. Decreasing the pitch and diameter ratio could increase the heat transfer rate. Moreover, it was demonstrated that the proposed innovative CRT outperformed both the ORT and PRT in terms of heat transfer performance. In the case of CRT, the highest number of teeth (N) offered the lowest friction factor and pressure drop.

Keywords: Heat transfer, numerical simulations, CFD, turbulators, finite volume method.

ENGINEERING JOURNAL Volume 26 Issue 8
Received 22 June 2021
Accepted 22 August 2022
Published 31 August 2022
Online at https://engj.org/
DOI:10.4186/ej.2022.26.8.13

DOI:10.4186/ej.2022.26.8.13

1. Introduction

Currently, heat exchanger tools have been applied to many applications. Therefore, increasing the heat transfer in heat exchangers has gained significant interest. In order to improve the heat transfer performance of heat exchangers, many research works have explored the use of a passive approach which does not need external power. A turbulator is one of the passive devices which has been studied. Described as a static mixer, turbulators are typically inserted into the heat exchanger tubes to help increase the tube-side heat transfer efficiency by inducing turbulent fluid flow. Their applications include, for example, in shell and tube heat exchangers, solar water heaters, boilers, tubular reactors and falling-film evaporators. Different turbulator geometries have been studied experimentally in different applications [1-12].

Among those being used, circular and conical ring turbulators have been observed over the last decade. Kongkaitpaiboon et al. [3] conducted an experimental study on the turbulent flow conditions in a plain tube with circular-ring and perforated conical-ring turbulators installed. The convective heat transfer and pressure loss were analyzed. Kumar et al. [4] experimentally investigated fluid flow behavior and heat transfer performance by using a heat exchanger with a solid hollow circular disk installed. From these studies, increasing heat transfer was found to be associated with decreasing the diameter ratio and pitch ratio. The experimental studies by Kongkaitpaiboon et al. [5] and Acır et al. [6] using perforated conical and circular ring turbulators showed that the increase in the perforated number was associated with a decrease in the pressure drop. Similarly, Muthusamy et al. [7] applied conical cut-out turbulators with internal fins in a circular tube and reported that it had high potential to decrease pressure drop. In addition, some other inserted geometries were investigated, such as V-nozzle turbulators [8], a combination of twisted tape with circular ring turbulators [9], twisted-ring turbulators [10], louver-type turbulators [11], flow divider-type turbulators [12] coiled wire [13, 14, 15], and fixed and rotating turbine-type swirl generators [16, 17].

Many researchers have applied numerical analysis to learn the effect of these additional devices on flow patterns and heat transfer in circular tubes. Date [18] reported fully developed and uniform flows in the twisted tape inserted tube using numerical investigation. The twisted tape was also studied by Ray and Date [19]. With peripherally and axially constant wall heat flux conditions, the periodic flow and heat transfer rate were predicted in a square duct with twisted tape insert. The effect of generated secondary flow in swirl tubes on the temperature field and heat transfer performance was investigated by Kazuhisa et al. [20]. The effect of gravity on the secondary flow transition process, flow pattern and the local Nusselt number under a uniform heat flux condition were also determined. Akansu [21] noticed the effects of the height and length ratios of porous-ring turbulators in a circular pipe on heat transfer and pressure drop. Pathipakka and Sivashanmugam [22] observed the heat transfer behavior of nanofluid flow in a ring-shaped tube fitted with helical inserts by varying the helical twist ratio under constant heat flux conditions. Oni and Paul [23] numerically investigated the flow characteristics and heat transfer of water flow with swirls induced by different twisted tapes in a circular tube. Ibrahim et al. [24] applied three arrangements of conical rings in a circular tube. From these studies, new correlations for Nusselt number, friction factor and enhancement efficiency have been proposed and compared with published works.

In this study, the innovative cogwheel-ring turbulator (CRT) was proposed to increase and improve heat transfer performance (η) in a plain tube. The gaps between the teeth of the cogwheel-ring turbulator were expected to reduce the pressure drop across the tube and produce recirculating flow. Computational fluid dynamics (CFD) was employed to study the effects of various parameters, i.e., diameter ratio (DR), pitch ratio (PR), the number of teeth in a cogwheel-ring turbulator (N), and Reynolds number (Re). Furthermore, the Nusselt number (Nu) and friction factor (f) obtained from the statistical correlations by using various types of ring-shaped turbulators were compared with the same findings from a circular tube without turbulators.

2. Model Geometries

The model geometries were constructed as a circular tube with different types of turbulators, including an orbicular-ring turbulator (ORT), a pyramidal-ring turbulator (PRT) and a proposed innovative cogwheel-ring turbulator (CRT). The tube was made from a 2 mm-thick copper material which possessed high thermal conductivity (k)(Fig. 1). The tube length (L) and internal diameter (D) were 1500 mm and 62 mm, respectively. The details of the three types of turbulators made with 5 mm-thick aluminum are demonstrated in Fig. 2. The turbulator outer diameter (D) was fixed at 62 mm while the diameter ratio ($DR = d/D$) was varied as 0.5, 0.6 and 0.7. The simulated pitch ratios ($PR = p/D$) were 4 and 8. The CRT with different numbers of teeth ($N = 6, 8$ and 10) by partial cut-out of PRT was considered.

3. Mathematical Model and Numerical Procedure

Mathematical models were developed to predict fluid flow and heat transfer behavior. Applying the conventional flow and energy equations for the heat transfer process modeling in a circular tube equipped with different turbulators, some simplifying assumptions are considered. The assumptions are: (1) the flow through the turbulators is incompressible and turbulent; (2) the steady state flow is in mean flow; and (3) the fluid properties are constant.

3.1. Governing Questions

The governing equations of turbulent and incompressible flow are the continuity, momentum and energy conservation equations. The equations are written in cylindrical coordinates as follows:

Continuity equation

$$\frac{\partial u_x}{\partial x}+\frac{1}{r}\frac{\partial}{\partial r}(ru_r)+\frac{1}{r}\frac{\partial u_\theta}{\partial \theta}=0 \tag{1}$$

Momentum conservation equation

x - Momentum:

$$\frac{\partial(\rho u_x u_x)}{\partial x}+\frac{1}{r}\frac{\partial(\rho r u_r u_x)}{\partial r}+\frac{1}{r}\frac{\partial(\rho u_\theta u_x)}{\partial \theta}-\frac{\partial}{\partial x}\left(\mu_e\frac{\partial u_x}{\partial x}\right)$$
$$-\frac{1}{r}\frac{\partial}{\partial r}\left(r\mu_e\frac{\partial u_x}{\partial r}\right)-\frac{\partial}{\partial \theta}\left(\mu_e\frac{\partial u_x}{\partial \theta}\right)=-\frac{\partial p}{\partial x}+\frac{\partial}{\partial x}\left(\mu_e\frac{\partial u_x}{\partial x}\right)$$
$$+\frac{1}{r}\frac{\partial}{\partial r}\left(r\mu_e\frac{\partial u_r}{\partial x}\right)+\frac{1}{r}\frac{\partial}{\partial \theta}\left(\mu_e\frac{\partial u_\theta}{\partial x}\right) \tag{2}$$

r - Momentum:

$$\frac{\partial(\rho u_x u_r)}{\partial x}+\frac{1}{r}\frac{\partial(\rho r u_r u_r)}{\partial r}+\frac{1}{r}\frac{\partial(\rho u_\theta u_r)}{\partial \theta}-\frac{\partial}{\partial x}\left(\mu_e\frac{\partial u_r}{\partial x}\right)$$
$$-\frac{1}{r}\frac{\partial}{\partial r}\left(r\mu_e\frac{\partial u_r}{\partial r}\right)-\frac{\partial}{\partial \theta}\left(\mu_e\frac{\partial u_r}{\partial \theta}\right)=-\frac{\partial p}{\partial r}+\frac{\partial}{\partial x}\left(\mu_e\frac{\partial u_x}{\partial r}\right)$$
$$+\frac{1}{r}\frac{\partial}{\partial r}\left(r\mu_e\frac{\partial u_r}{\partial r}\right)-2\mu_e\left(\frac{u_r}{r^2}\right)+\frac{1}{r}\frac{\partial}{\partial \theta}\left(\mu_e\frac{\partial u_\theta}{\partial r}\right) \tag{3}$$

θ - Momentum:

$$\frac{\partial(\rho u_x u_\theta)}{\partial x}+\frac{1}{r}\frac{\partial(\rho r u_r u_\theta)}{\partial r}+\frac{1}{r}\frac{\partial(\rho u_\theta u_\theta)}{\partial \theta}-\frac{\partial}{\partial x}\left(\mu_e\frac{\partial u_\theta}{\partial x}\right)$$
$$-\frac{1}{r}\frac{\partial}{\partial r}\left(r\mu_e\frac{\partial u_\theta}{\partial r}\right)-\frac{\partial}{\partial \theta}\left(\mu_e\frac{\partial u_\theta}{\partial \theta}\right)=-\frac{\partial p}{\partial \theta}+\frac{\partial}{\partial x}\left(\mu_e\frac{\partial u_x}{\partial \theta}\right)$$
$$+\frac{1}{r}\frac{\partial}{\partial r}\left(r\mu_e\frac{\partial u_r}{\partial \theta}\right)-2\mu_e\left(\frac{u_\theta}{r^2}\right)+\frac{1}{r}\frac{\partial}{\partial \theta}\left(\mu_e\frac{\partial u_\theta}{\partial \theta}\right) \tag{4}$$

The velocity components u_x, u_r and u_θ are the velocity components of axial (x), radial (r) and azimuthal (θ) directions, and μ_e is the effective viscosity which is the sum of the laminar viscosity (μ_l) and the turbulent viscosity (μ_t)

$$\mu_e=\mu_l+\mu_t \tag{5}$$

Energy conservation equation:

$$\frac{1}{r}\left[\frac{\partial}{\partial x}(r\rho u_x T)+\frac{\partial}{\partial r}(r\rho u_r T)+\frac{\partial}{\partial \theta}(r\rho u_\theta T)\right]$$
$$=\frac{1}{r}\left[\frac{\partial}{\partial x}\left(r\frac{\mu_e}{\sigma_T}\frac{\partial T}{\partial x}\right)+\frac{\partial}{\partial r}\left(r\frac{\mu_e}{\sigma_T}\frac{\partial T}{\partial r}\right)+\frac{\partial}{\partial \theta}\left(r\frac{\mu_e}{\sigma_T}\frac{\partial T}{\partial \theta}\right)\right] \tag{6}$$

where σ_T is the turbulent Prandtl number at constant temperature.

3.2. The Standard $k-\varepsilon$ Model

The standard model [25] employed in this work is a two-equation turbulence model. Although it does not perform well in the prediction of various flow systems with large extra strains (e.g. curved boundary layers, strong streamline curvature, swirling flows and rotating flows) compared with some turbulence models such as the Renormalized Group (RNG) model, the standard $k-\omega$ model and the Shear Stress Transport (SST) $k-\omega$ model [26-28], it has advantages in terms of the aspects of simplicity, robustness and reasonable accuracy for a wide range of turbulent flow measurements. Over the past decades, it has been the most widely used and validated turbulence model [29-31] and it has been applied in many systems [32-36]. The standard $k-\varepsilon$ model is still extensively utilized for the basic calculation of turbulence models in the applications of fluid flows. It can also drastically reduce the computing time and memory data during the simulations compared to other models [37].

The variants of the turbulent flow characteristics for kinetic energy (k) and dissipation rate (ε) are used to define the length scale (ℓ) and velocity scale (ϑ), which represent the large-scale turbulence as follows:

$$\ell=\frac{k^{3/2}}{\varepsilon} \tag{7}$$

$$\vartheta=k^{3/2} \tag{8}$$

by applying dimensional analysis, we can specify the turbulent viscosity as:

$$\mu_t=C\rho\vartheta\ell=\rho C_\mu\frac{k^2}{\varepsilon} \tag{9}$$

where C_μ is a dimensionless constant.

The standard $k-\varepsilon$ model uses the following transport equations for k and ε given as:

$$\frac{1}{r}\left(\frac{\partial}{\partial x}(r\rho u_x k)+\frac{\partial}{\partial r}(r\rho u_r k)+\frac{\partial}{\partial \theta}(r\rho u_\theta k)\right)+\left(\frac{\partial}{\partial x}\left(r\left(\mu_l+\frac{\mu_t}{\sigma_k}\right)\frac{\partial k}{\partial x}\right)\right)$$
$$+\frac{1}{r}\left(\frac{\partial}{\partial r}\left(r\left(\mu_l+\frac{\mu_t}{\sigma_k}\right)\frac{\partial k}{\partial r}\right)\right)+\frac{1}{r}\left(\frac{\partial}{\partial \theta}\left(r\left(\mu_l+\frac{\mu_t}{\sigma_k}\right)\frac{\partial k}{\partial \theta}\right)\right)=G-\rho\varepsilon \tag{10}$$

Dissipation rate of turbulent kinetic energy equation:

$$\frac{1}{r}\left(\frac{\partial}{\partial x}(r\rho u_x\varepsilon)+\frac{\partial}{\partial r}(r\rho u_r\varepsilon)+\frac{\partial}{\partial \theta}(r\rho u_\theta\varepsilon)\right)$$
$$+\left(\frac{\partial}{\partial x}\left(r\left(\mu_l+\frac{\mu_t}{\sigma_\varepsilon}\right)\frac{\partial \varepsilon}{\partial x}\right)\right)+\frac{1}{r}\left(\frac{\partial}{\partial r}\left(r\left(\mu_l+\frac{\mu_t}{\sigma_\varepsilon}\right)\frac{\partial \varepsilon}{\partial r}\right)\right)$$
$$+\frac{1}{r}\left(\frac{\partial}{\partial \theta}\left(r\left(\mu_l+\frac{\mu_t}{\sigma_\varepsilon}\right)\frac{\partial \varepsilon}{\partial \theta}\right)\right)=\frac{\varepsilon}{k}\left(C_{\varepsilon 1}G-C_{\varepsilon 2}\rho\varepsilon\right) \tag{11}$$

where G is the turbulent energy production rate and can be calculated as follows:

DOI:10.4186/ej.2022.26.8.13

$$\frac{G}{\mu_t}=2\left[\left(\frac{\partial u_x}{\partial x}\right)^2+\left(\frac{\partial u_r}{\partial r}\right)^2+\left(\frac{u_r}{r}\right)^2+\left(\frac{\partial u_\theta}{\partial \theta}\right)^2+\left(\frac{u_\theta}{\theta}\right)^2\right]$$
$$+\left(\frac{\partial u_x}{\partial x}+\frac{\partial u_r}{\partial r}+\frac{\partial u_\theta}{\partial \theta}\right)^2 \quad (12)$$

The standard $k-\varepsilon$ model employs the values of the constants obtained by comprehensive data fitting for a wide range of turbulent flows ($C_\mu=0.09$, $\sigma_k=1.00$, $\sigma_\varepsilon=1.30$, $C_{\varepsilon 1}=1.44$ and $C_{\varepsilon 2}=1.92$) [38].

Table 1. List of boundary conditions

Boundary	Conditions
Inlet	Velocity: $\mathrm{Re}=\frac{\varrho u_m D_h}{\mu}$ Turbulent intensity: $I=0.16\mathrm{Re}^{-0.125}$
Outlet	Zero-gauge pressure gradients: $\left.\frac{\partial P}{\partial x}\right\|_{exit}=0$
Wall surface	No-slip wall condition: $u_i=0$ Uniform wall heat flux condition: $-k\left.\frac{\partial T}{\partial r}\right\|_{\text{fluid}}=q''$

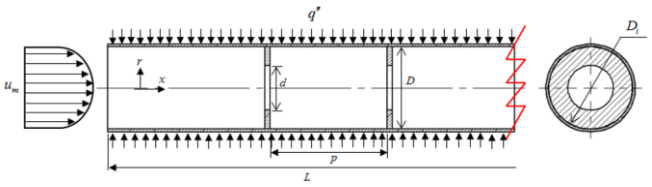

Fig.1. Test section of a circular tube equipped with ring-shaped turbulators operated under uniform wall heat flux.

(a)

(b)

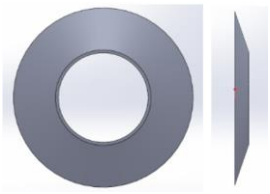

(c)

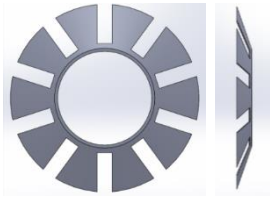

Fig. 2. Types of turbulator (a) Orbicular-ring turbulator (ORT), (b) Pyramidal-ring turbulator (PRT), (c) Cogwheel-ring turbulator (CRT) with $N=10$.

3.3. Solution Procedure

For the 3D numerical simulation, the commercial software of ANSYS FLUENT VERSION 15.0 was used. The Reynolds-averaged Navier-Stokes equations for time independent and incompressible flow and the turbulence model were confirmed to be prudent by using a finite volume method. The QUICK scheme [39] was applied for convection and diffusion terms. The pressure-velocity coupling algorithm SIMPLE and TDMA [40] were selected to evaluate the pressure and velocity fields. The solution was considered convergent when the difference between the normalized residual of the algebraic equation and the prescribed value was less than 10^{-4}.

In the current work, three parameters of interest for the characterization of heat transfer, friction loss, and efficiency of heat transfer improvement in the circular tube fitted with turbulators were: (1) Nusselt number; (2) friction factor; and (3) heat transfer performance, respectively.

The Nusselt number, Nu, is defined as:

$$\mathrm{Nu}=\frac{hD_h}{k} \quad (13)$$

For the plain tube with ring-shaped turbulators, the hydraulic diameter (D_h) is equivalent to the internal diameter of the plain tube (D). The friction factor (f) is calculated from the pressure drop:

$$\Delta P=f\frac{L}{D}\frac{u_m^2}{2}\varrho \quad (14)$$

The Nusselt number and friction factor for a fully developed turbulent flow condition in a plain tube were used as the base data for evaluating performance. The Dittus-Boelter correlation [41] for the Nusselt number in the smooth tube is:

$$\mathrm{Nu}=0.023\mathrm{Re}^{0.8}\,\mathrm{Pr}^{0.4} \quad (15)$$

The Blasius correlation [42] for the friction factor in the smooth tube is:

$$f=0.316\mathrm{Re}^{-0.25};3000<\mathrm{Re}<20{,}000 \quad (16)$$

Finally, the heat transfer performance representing the efficiency of heat transfer improvement in the plain tube

fitted with various types of turbulators can be calculated by the Webb correlation [43] as follows:

$$\eta = \left(\frac{\mathrm{Nu}_t}{\mathrm{Nu}_p}\right)\left(\frac{f_t}{f_p}\right)^{-\frac{1}{3}} \quad (17)$$

where Nu_p, f_p, Nu_t and f_t are the Nusselt numbers and friction factors for the plain tube and the tube equipped with ring-shaped turbulators, respectively.

4. Fluid Properties and Boundary Conditions

All the thermal physical properties of the air are evaluated at 300 K [44]. These properties are density (ϱ), specific heat (C_p), thermal conductivity (k) and dynamic viscosity (μ) of 1.1765 kg/m^3, 1006.3 J/kg.K, 0.02612 W/m.K and 0.000018538 kg/m.s, respectively [32]. The RANS equations and transport equations were subjected to the boundary conditions as summarized in Table 1. The air flows were set at a constant temperature of 300 K, and the Reynolds numbers were in the range of 4,000 to 20,000 at the inlet boundaries. The outlet boundaries were specified as a zero-gauge pressure. No-slip condition and 3,500 W/m^2 uniform wall heat-flux (q'') were applied on the inner and outer tube walls, respectively.

Table 2. Details of grid independence.

Case	Type	*DR*	*PR*	Grid size (mm)	No. of cell
1	ORT	0.5	4	4.5	559,315
2	ORT	0.5	4	4	623,489
3	ORT	0.5	4	3	1,184,996

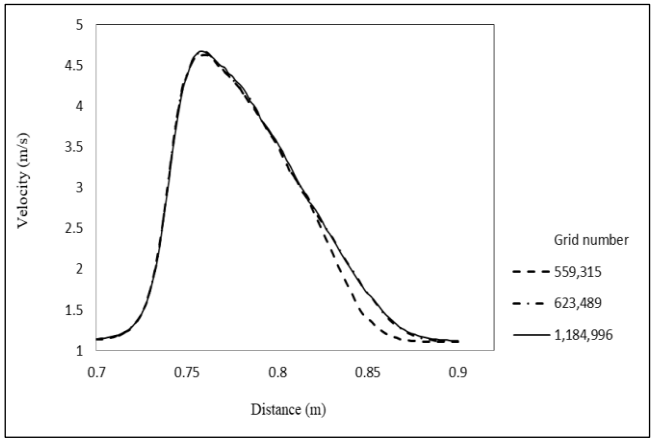

Fig. 3. Velocity across the longitudinal section at the exit of ORT for different grids at Re = 20,000.

(a)

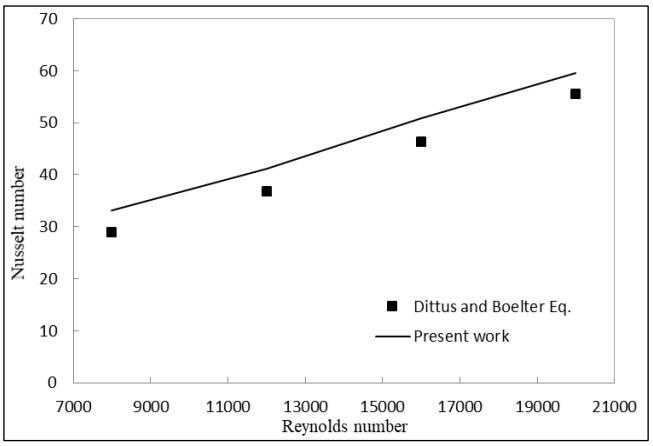

(b)

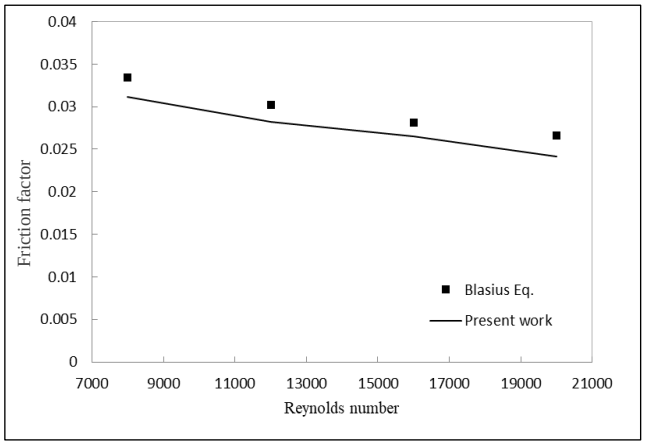

Fig. 4. Comparison of the Nusselt number with the correlations calculated from (a) Dittus and Boelter equation [41], (b) Blasius equation [42].

5. Grid Independence and Validation Tests

A grid independence test was conducted to confirm the numerical solution accuracy. The equipped-ORT tube with *DR* = 5 and *PR* = 4 was simulated by using three grid sizes as given in Table 2. Velocities across the longitudinal section at the exit of different grid sizes at Re = 20,000 were plotted as shown in Fig. 3. Insignificant differences between the results obtained by using 623,489 and 1,184,996 grid cells were observed. Therefore, the total number of grid cells used for calculating the flows was 623,489.

For the numerical simulation's validation, the Nusselt number and friction factor were obtained by using the standard $k-\varepsilon$ model for the plain tube and the tube equipped with orbicular-ring turbulator (ORT) compared with the established correlations and experimental results. The variables of friction factor and Nusselt number results for the circular tube case were identified with Dittus and Boelter correlation [41] and Blasius correlation [42]. For

DOI:10.4186/ej.2022.26.8.13

the ORT, the simulation results were verified with the experimental results from Kongkaitpaiboon et al. [3]. The plain tube validation results are presented in Fig. 4. The present simulation results concur with the published correlation results. The simulated Nusselt numbers and friction factors show maximum deviations of 5.74% (Fig. 4 (a)) and 4.38% (Fig. 4 (b)), respectively. The ORT validation results as depicted in Fig. 5 indicate that the Nusselt numbers are in good agreement with the experimental results [3] and show a maximum deviation of 1.33% (Fig. 5 (a)). In addition, the friction factor results also agree well with 1.74% maximum deviation (Fig. 5 (b))

(a)

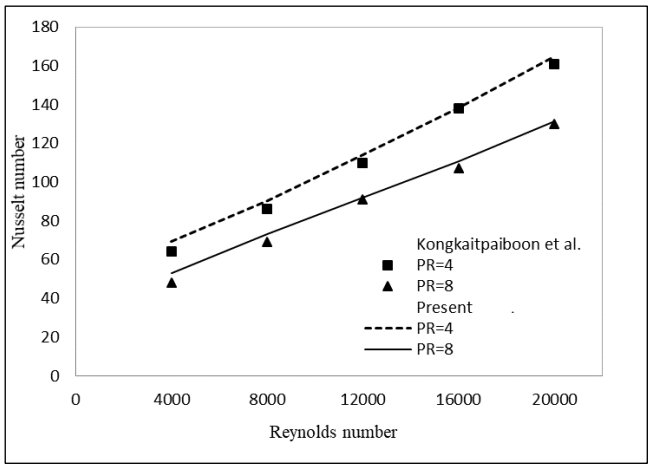

(b)

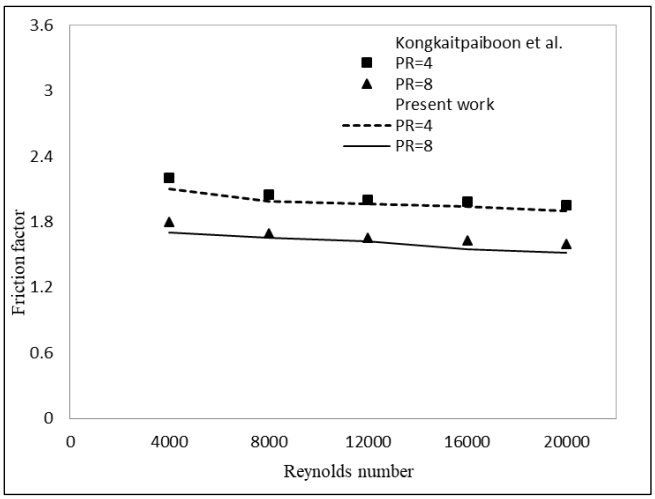

Fig. 5. Comparison between the present numerical simulations and the experiments by Kongkaitpaiboon et al. [3] for ORT (a) Nusselt number, and (b) friction factor.

6. Numerical Results

6.1. Velocity Vectors and Streamlines

The velocity vectors for the ORT-equipped tube with fixed pitch ratio ($PR = 4$) and Reynolds number (Re = 20,000) were plotted at different diameter ratios (DR) as shown in Fig. 6 (a – c). It can be observed that vortices appeared behind the turbulators. A low pressure area was created immediately at the flow downstream of the turbulators. The fluid partially flows into this area separated from the main flow resulting in an induced recirculating flow. This recirculation area became smaller when the diameter ratio was increased from 0.5 to 0.7. The vector plots for PRT and CRT cases were also investigated as shown in Fig. 6 (d – e). The PRT and ORT provided similar results, whereas the use of CRT could remove the recirculation region for all diameter ratios (DR) and the number of CRT channels.

The streamline plots of the three turbulator types at $DR = 0.7$, $PR = 4$ and Re = 20,000 are displayed in Fig. 7. It is clearly seen that for the CRT, there is no recirculation region behind the turbulator, which is different from the ORT and PRT cases. Figure 7 (d) shows the three-dimensional view of the flow in the CRT tube. However, the smallest recirculating flow is clearly observed at the cogwheel teeth spaces.

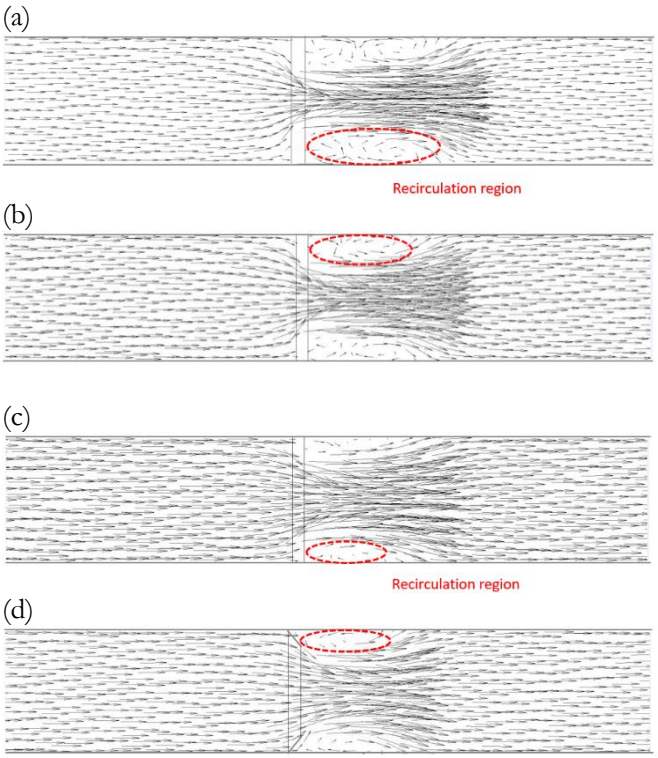

Fig. 6. Velocity vector plots at different diameter ratios (DR) with fitted pitch ratio ($PR = 4$) for ORT (a) DR = 0.5, (b) DR = 0.6, (c) DR = 0.7; for PRT, (d) DR = 0.7 and for CRT, (e) DR = 0.7 and N = 6.

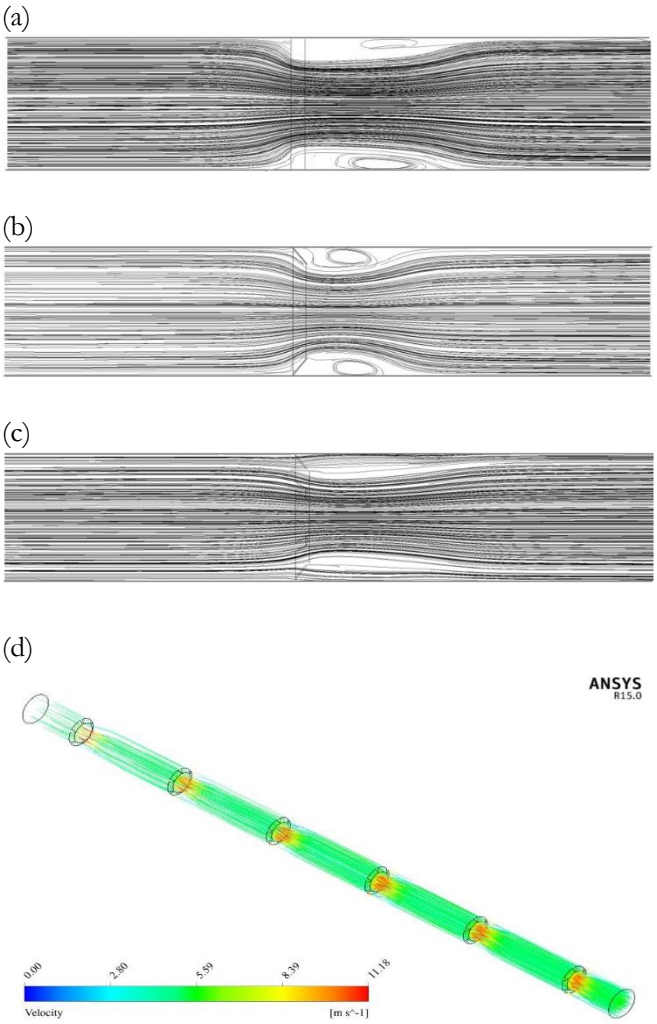

Fig. 7. Streamline contour plots for tubes with different types of turbulators (a) Orbicular-ring (ORT), (b) Pyramidal-ring (PRT), (c) Cogwheel-ring (CRT), (d) Cogwheel-ring (CRT) (3D).

6.2. Static Pressure

Static pressure contours in the tubes fitted with different types of turbulators with $DR = 0.7$, $PR = 4$ and Re = 20,000 are demonstrated in Fig. 8. High pressure drops were found when fluid flowed across the turbulators along the tube length. The PRT showed the highest pressure drop (552.9 Pa) while the CRT offered the lowest at 344.12 Pa. For CRT, the pressure drop was increased in line with decreases in the number of channels (N).

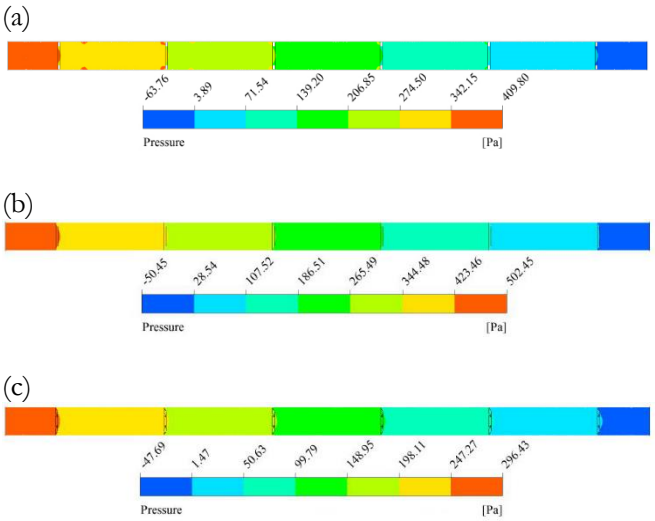

Fig. 8. Static pressure contour plots for tubes with different types of turbulator (a) Orbicular ring (ORT), (b) Pyramidal-ring (PRT), (c) Cogwheel-ring (CRT)

6.3. Temperature Field

The temperature profiles of the circular tubes equipped with different types of ring-shaped turbulators with $DR = 0.7$, $PR = 4$ and Re = 20,000 are shown in a contour plot (Fig. 9). The temperatures rose from the inlet to the outlet due to heat transfer from the wall to the fluid. The highest temperature was found at the wall near the exit of the plain tube. The ORT and PRT cases showed lower values for the highest temperature than the CRT because the heat transfer from the wall was enhanced at the recirculation region.

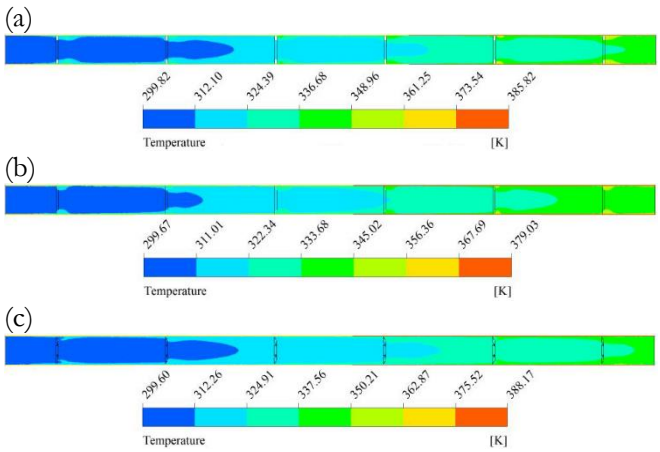

Fig. 9. Temperature contour plots for tubes with different types of turbulators (a) Orbicular ring (ORT), (b) Pyramidal-ring (PRT), (c) Cogwheel-ring (CRT).

DOI:10.4186/ej.2022.26.8.13

6.4. Heat Transfer

The influence of the turbulators on the heat transfer is indicated in Fig. 10. The Nusselt numbers in the tubes with different turbulators at $DR = 0.5$ and $PR = 4$ were plotted against the Reynolds numbers. The heat transfer enhancement was amplified at a higher Reynolds number since the convective heat transfer was more effectively promoted at a higher turbulence level. The flows in tubes fitted with tabulators showed higher convective heat transfer than was observed in the plain tube. The CRT can offer higher heat transfer by 73–143% of those in the plain tube but the Nusselt numbers are lower than those in the ORT and PRT by a range of 15–18%. The simulation results also reveal that the Nusselt numbers increased with decreases in the *DR*, *PR* and *N*. It can be explained that when the *DR*, *PR* and *N* were smaller, there was more flow blockage, and thus stronger turbulence intensity.

6.5. Friction Factor

The friction factor characteristics of the tubes with PRT and CRT are illustrated in Fig. 11. The calculated friction factors of the tubes with CRT at $DR = 0.7$ and $PR = 8$ are 28%–74% of the PRT factors. The friction factors are related to the friction areas. The partial cutting out of the CRT minimizes the friction areas and factors. The friction factor decreased in line with the incremental increases in the Reynolds number *DR*, *PR* and *N* and it was inversely proportional to the square of the flow velocity. The minimum was found in the tube with CRT. In addition, it may be seen that the friction factors at different numbers of channels (*N*) are slightly different.

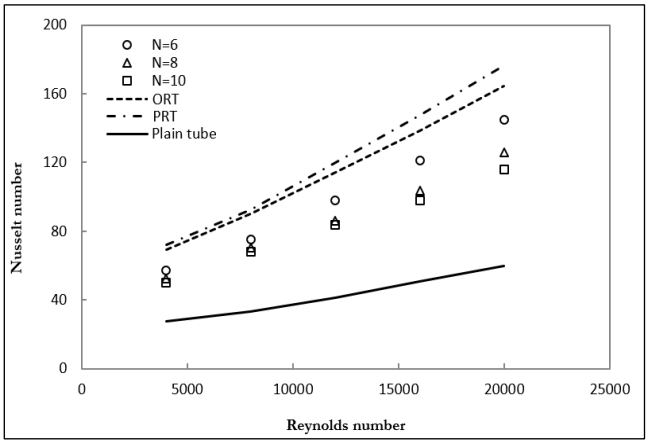

Fig. 10. Relationship between the Nusselt numbers and Reynolds numbers.

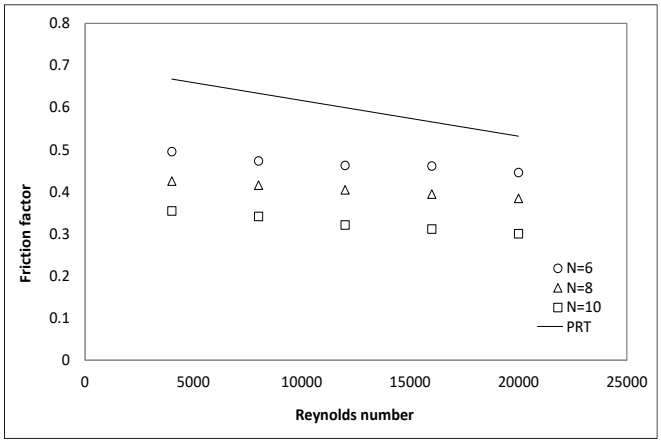

Fig. 11. Relationship between the friction factors and Reynolds numbers.

6.6. Heat Transfer Performance

Figure 12 shows that for all turbulator cases, the heat transfer performance tended to decrease when the Reynolds number increased. The *DR* was varied at $PR = 4$. However, it is clearly seen that $DR = 0.7$ provides the best performance. The CRT with $N = 6$ has a heat transfer performance of 1.21–1.42 times over that of the ring-shaped tube. Figure 13 compares the heat transfer performance of the tubes (η_t) with three turbulator types ($DR = 0.7$ and $PR = 4$) calculated using an equation similar to the Webb equation [43]. The performance indicates the efficiency of turbulators for the enhancement of heat transfer. The performances which are the relation between the Nusselt numbers and the friction factors are shown as constant curves of heat transfer performance in the range of 60–200%. The results show that the tube with CRT provided the highest heat transfer performance and the tube with ORT gave the lowest heat transfer performance. It also reveals that the case of CRT with $DR = 0.7$, $PR = 4$ and $N = 6$ at Re = 20,000 produced the highest heat transfer performance, which was 185% higher than the others. In the same case with Re = 20,000, the highest results for the PRT and the ORT are 175% and 164%. Although CRT did not show any recirculation, this design provided the highest heat transfer performance and could decrease pressure drop significantly. Therefore, this case is the suitable design for reliable operation in this operating range.

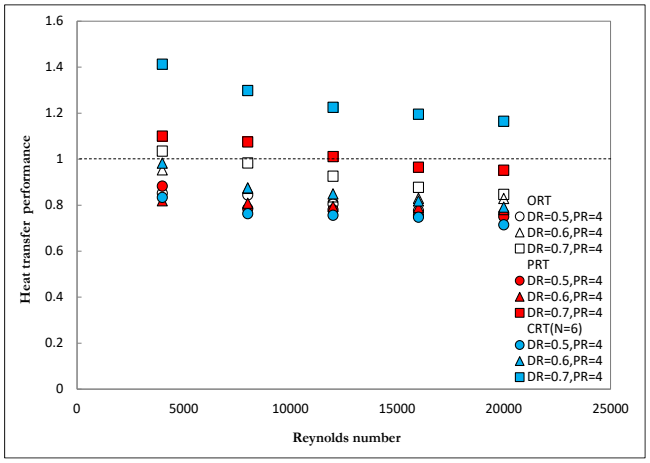

Fig. 12. Relationship between the heat transfer performances and Reynolds numbers.

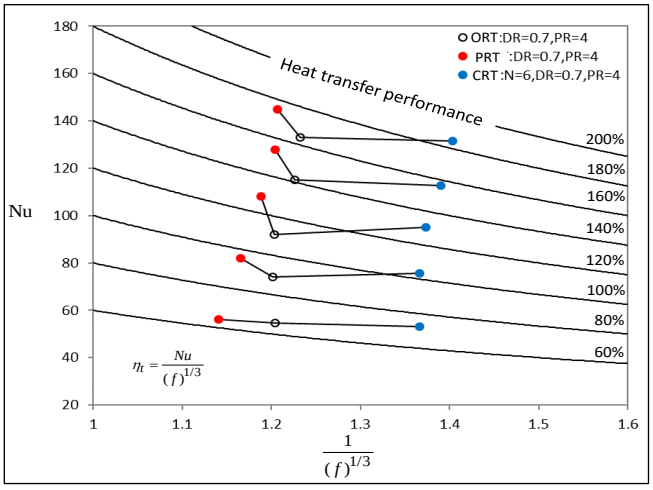

Fig. 13. Comparison of heat transfer performance for the various types of turbulators.

7. Conclusions

Numerical investigation using the standard $k-\varepsilon$ model was conducted to measure air flow through circular tubes equipped with different ring-shaped turbulators (ORT, PRT and CRT) in order to study heat transfer and flow characteristics. The influences of the diameter and pitch ratios on the heat transfer rate, friction factor and thermal performance factor behaviors were investigated under a uniform wall heat flux condition. The numerical method was validated with the experimental results reported in the literature and the established correlations, and good agreement was observed. From the simulation results, the heat transfer rates in the tube equipped with ORTs and PRTs are 87% to 199% higher than that of the tube without turbulators due to the recirculation. For CRT, the highest heat transfer performance was 1.42 times over that of the plain tube. The CRT also offered the lowest pressure drop.

Acknowledgement

This research was supported by Ratchadapisaek Sompote Endowment under Outstanding Research Performance Program and the Thailand Research Fund (DPG5880003). The second and third authors also would like to acknowledge Ratchadapisaek Sompote Fund Post-Doctoral Support from Chulalongkorn University.

References

[1] K. Yakut and B. Sahin, "Flow-induced vibration analysis of conical rings used for heat transfer enhancement in heat exchangers," *Appl. Energy*, vol. 78, no. 3, pp. 273-288, 2004.

[2] K. Yakut, B. Sahin, and S. Canbazoglu, "Performance and flow-induced vibration characteristics for conical-ring turbulators," *Appl. Energy*, vol. 79, no. 1, pp. 65-76, 2004.

[3] V. Kongkaitpaiboon, K. Nanan, and S. Eiamsa-ard, "Experimental investigation of convective heat transfer and pressure loss in a round tube fitted with circular-ring turbulators," *Int Commun Heat Mass*, vol. 37, no. 5, pp. 568-574, 2010.

[4] A. Kumar, S. Chamoli, and M. Kumar, "Experimental investigation on thermal performance and fluid flow characteristics in heat exchanger tube with solid hollow circular disk inserts," *Appl. Therm. Eng.*, vol. 100, pp. 227-236, 2016.

[5] V. Kongkaitpaiboon, K. Nanan, and S. Eiamsa-ard, "Experimental investigation of heat transfer and turbulent flow friction in a tube fitted with perforated conical-rings," *Int Commun Heat Mass*, vol. 37, no. 5, pp. 560-567, 2010.

[6] A. Acır, İ. Ata, and M. E. Canlı, "Investigation of effect of the circular ring turbulators on heat transfer augmentation and fluid flow characteristic of solar air heater," *Exp Therm Fluid Sci.*, vol. 77, pp. 45-54, 2016.

[7] C. Muthusamy, M. Vivar, I. Skryabin, and K. Srithar, "Effect of conical cut-out turbulators with internal fins in a circular tube on heat transfer and friction factor," *Int Commun Heat Mass*, vol. 44, pp. 64-68, 2013.

[8] S. Eiamsa-ard and P. Promvonge, "Experimental investigation of heat transfer and friction characteristics in a circular tube fitted with V-nozzle turbulators," *Int Commun Heat Mass*, vol. 33, no. 5, pp. 591-600, 2006.

[9] P. Promvonge and S. Eiamsa-ard, "Heat transfer behaviors in a tube with combined conical-ring and twisted-tape insert," *Int Commun Heat Mass*, vol. 34, no. 7, pp. 849-859, 2007

[10] C. Thianpong, K. Yongsiri, K. Nanan and S. Eiamsa-ard, "Thermal performance evaluation of heat exchangers fitted with twisted-ring turbulators," *Int Commun Heat Mass*, vol. 39, no. 6, pp. 861-868, 2012.

[11] T. M. Liou, S. W. Chang, and S. P. Chan, "Experimental study on thermal flow characteristics in square serpentine heat exchangers mounted with louver-type turbulators," *Int J Heat Mass Tran*, vol. 116, pp. 897-908, 2018.

[12] S. P. Nalavade, C. L. Prabhune, and N. K. Sane, "Effect of novel flow divider type turbulators on fluid flow and heat transfer," *Ther. Sci. Eng. Prog.*, vol. 9, pp. 322-331, 2019.

[13] M. A. Akhavan-Behabadi, M. R. Salimpour, and V. A. Pazouki, "Pressure drop increase of forced convective condensation inside horizontal coiled wire inserted tubes," *Int Commun Heat Mass*, vol. 35, no. 9, pp.1220-1226, 2008.

[14] T. Sukchana, "Heat transfer enhancement of the double pipe heat exchanger with wire Inserts," M.S. thesis, ME Dept., Srinakharinwirot University, Nakhon Nayok, 2009.

[15] S. Khorasani, S. Jafarmadar, S. Pourhedayat, M.A.A. Abdollahi, and A. Heydarpour, "Experimental investigations on the effect of geometrical properties of helical wire turbulators on thermal performance of a helically coiled tube," *Appl. Therm. Eng.*, Vol. 147, pp. 983-990, 2019.

[16] W. Duangthongsuk and S. Wongwises, "An experimental investigation of the heat transfer and pressure drop characteristics of a circular tube fitted with rotating turbine-type swirl generators," *Exp Therm Fluid Sci.*, vol. 45, pp. 8-15, 2013.

[17] W. Duangthongsuk and S. Wongwises, "Comparison of the heat transfer performance and friction characteristics between fixed and rotating turbine-type swirl generators fitted in a small circular tube," *Exp Therm Fluid Sci.*, vol. 50, pp. 222-228, 2013.

[18] A. W. Date, "Prediction of fully developed flow in a tube containing a twisted tape," *Int J Heat Mass Tran*, vol. 17, pp. 845-859, 1974.

[19] S. Ray and A. W. Date, "Laminar flow and heat transfer through square duct with twisted tape insert," *Int J Heat Mass Tran*, vol. 22, pp. 460-472, 2001.

[20] Y. Kazuhisa, H. Hidetoshi, T. Saburo, and S. Chikahiro, "Numerical simulation on heat transfer enhancement in twisted-tape-inserted tubes," *Journal of Enhanced Heat Transfer*, vol. 11, pp. 379-389, 2004.

[21] S. O. Akansu, "Heat transfers and pressure drops for porous-ring turbulators in a circular pipe," *Appl. Energy*, vol. 83, pp. 280- 298, 2006.

[22] G. Pathipakka and P. Sivashanmugam, "Heat transfer behavior of nanofluids in a uniformly heated circular tube fitted with helical inserts in laminar flow," *Superlattices and Microstructures*, vol. 47, no. 2, pp. 349-360, 2010.

[23] T. O. Oni and M. C. Paul, "Numerical investigation of heat transfer and fluid flow of water through a circular tube induced with divers' tape inserts," *Appl. Therm. Eng.*, vol. 98, pp. 157-168.

[24] M. M. Ibrahim, M. A. Essa, and N. H. Mostafa, "A computational study of heat transfer analysis for a circular tube with conical ring turbulators," *Int. J. Therm. Sci.*, vol. 137, pp. 138-160, 2019.

[25] B. E. Launder and D. B. Spalding, "The numerical computation of turbulent flows," *Comput Method Appl M*, vol. 3, pp. 269-289, 1974.

[26] V. Yakhot and S. A. Orszag, "Renormalisation group analysis of turbulence; basic theory," *J. Sci. Comput.*, vol. 1, pp. 3-51, 1986.

[27] D. C. Wilcox, "Reassessment of the scale-determining equation for advanced turbulence models," *AIAA Journal*, vol. 26, no. 11, pp. 1299-1310, 1988.

[28] F. R. Menter, "Two-equation Eddy-viscosity turbulence models for engineering applications," *AIAA Journal*, vol. 32, no. 8, pp. 1598-1605, 1994.

[29] C. G. Speziale, "On non-linear $k-\omega$ and $k-\varepsilon$ models of turbulence," *J. Fluid Mech*, vol. 178, pp. 459-475, 1987.

[30] V. Yakhot, S. A. Orszag, S. Thangam, T. B. Gatski and C.G. Speziale, "Development of turbulence models for shear flows by a double expansion technique," *Phys. Fluids*, vol.4, pp. 1510-1520, 1992.

[31] M. Tsuchiya, S. Murakami, A. Mochida, K. Kondo and Y. Ishida, "Development of a new $k-\varepsilon$ model for flow and pressure fields around bluff body," *J. Wind Eng. Ind. Aerodyn.*, vol. 67&68, pp. 169-182, 1997.

[32] N. F. Aljuwayhel, G. F. Nellis, and S. A. Klein, "Parametric and internal study of the vortex tube using a CFD model," *Int J Refrig*, vol. 28, pp. 442-450, 2005.

[33] S. Eiamsa-ard and P. Promvonge, "Numerical study on heat transfer of turbulent channel flow over periodic grooves," *Int Commun Heat Mass,* vol. 35, pp. 442-450, 2005.

[34] L. H. Tang, M. Zeng, and Q. W. Wang, "Experimental and numerical investigation on air-side performance of fin-and-tube heat exchangers with various fin patterns," *Exp Therm Fluid Sci,* vol. 33, pp. 818-827, 2009.

[35] E. Ozden and I. Tari, "Shell side CFD analysis of a small shell-and-tube heat exchanger," *Energy Convers. Manag.*, vol. 51, pp. 1004-1014, 2010.

[36] P. Wang, D. Y. Liu, and C. Xu, "Numerical study of heat transfer enhancement in the receiver tube of direct steam generation with parabolic trough by inserting metal foams," *Appl. Energy*, vol. 102, pp. 449-460, 2013.

[37] V. Kumar, S. Saini, M. Sharma, and K. D. P. Nigam, "Pressure drop and heat transfer study in tube-in-tube helical heat exchanger," *Chem. Eng. Sci.*, vol. 61, pp. 4403-4416, 2006.

[38] H. K. Versteeg and W. Malalasekera, "An introduction to Computational Fluid Dynamics" in *The Finite Volume Method*, 2nd ed. Harlow, Essex England: Pearson Education Limited, 2007.

[39] B. P. Leonard, "A stable and accurate convective modeling procedure based on quadratic upstream

interpolation," *Comput Method Appl M,* vol. 19, pp. 59-98, 1979.
[40] S. V. Patankar, "Numerical heat transfer and fluid flow," in *Computational Methods in Mechanics and Thermal Sciences*. New York: Hemisphere Publishing, 1980.
[41] F. W. Dittus and L. M. K. Boelter, "Heat transfer in automobile radiator of the tubular type," *Int J Heat Mass Tran*, vol. 12, pp. 3-22, 1985.
[42] R. W. Fox and A. T. McDonald, *Introduction to Fluid Mechanics*, 8th ed. River Street, NJ, USA: John Wiley & Sons Inc., 2011.
[43] R. L. Webb, *Principles of Enhanced Heat Transfer*, 1st ed. NY, USA: John Wiley & Sons Inc., 1992.
[44] W. M. Kays and M. E. Crawford, *Convective Heat and Mass Transfer*, 2nd ed., New York: McGraw-Hill, 1980.

Chotitach Jitbumrung was born in Bangkok, Thailand on March 4, 1991. He received a B.Eng. from the Faculty of Engineering, Department of Mechanical Engineering, Srinakharinwirot University, Nakorn Nayok, Thailand, in 2013. In addition, he has gained experience in the characteristics of heat transfer and fluid flow especially air conditioning design from the National Metal and Materials Technology Center (MTEC). He completed his Master of Engineering in Mechanical Engineering, Faculty of Engineering, Chulalongkorn University, Bangkok, Thailand in 2017.

He was an accredited consultant with the Ministry of Energy in 2017. From 2017 to 2020, he was a process development and integration engineer in the Department of Research and Development (R&D), Seagate Technology Ltd. (Thailand). Since 2020, he has been a process development engineer with the Business Unit of Fiber Semiconductors Customer, Fabrinet Co., Ltd (Thailand).

Chayanoot Kositanont received her B.Eng. and D.Eng. degrees in Chemical Engineering from Chulalongkorn University, Thailand, in 2005 and 2013, respectively. From 2005 to 2008, she was a system engineer at Yokogawa (Thailand) Ltd. From 2014 to 2016, she was a project analyst and senior project analyst with the National Science and Technology Development Agency (NSTDA).

At present, she is a researcher of the Innovative Rubber Manufacturing Research Group at the National Metal and Materials Technology Center (MTEC), a member of NSTDA.

Suttichai Assabumrungrat is a professor at the Department of Chemical Engineering, Faculty of Engineering, Chulalongkorn University, Bangkok, Thailand. He received his B.Eng. degree from Chulalongkorn University, and his M.Sc. and Ph.D. degrees from Imperial College London.

His research interest is process intensification with a particular focus on multifunctional reactors.

Sompong Putivisutisak received his B.Eng. from Chulalongkorn University, and his M.Sc. and Ph.D. degrees in Advanced Mechanical Engineering from Imperial College London. Since 1999, he has been a faculty member at the Department of Mechanical Engineering, Chulalongkorn University.

At present, he is an associate professor and Head of the Advanced Computational Fluid Dynamics Research Unit, Chulalongkorn University. His research interest is computational fluid dynamics and turbulence modeling with particular focus on energy conversion and multifunctional reactors.